Development of three-dimensional collagen scaffolds with controlled architecture for cell migration studies using breast cancer cell lines

Jonathan J. Campbell [a, 1, 2], Anke Husmann [a, *, 2], Robert D. Hume [b, 2], Christine J. Watson [b], Ruth E. Cameron [a]

[a] Cambridge Centre for Medical Materials, Department of Materials Science and Metallurgy, University of Cambridge, Cambridge CB3 0FS, UK
[b] Department of Pathology, University of Cambridge, Cambridge, CB2 1QP, UK

ARTICLE INFO

ABSTRACT

Cancer is characterized by cell heterogeneity and the development of 3D *in vitro* assays that can distinguish more invasive or migratory phenotypes could enhance diagnosis or drug discovery. 3D collagen scaffolds have been used to develop analogues of complex tissues *in vitro* and are suited to routine biochemical and immunological assays. We sought to increase 3D model tractability and modulate the migration rate of seeded cells using an ice-templating technique to create either directional/anisotropic or non-directional/isotropic porous architectures within cross-linked collagen scaffolds. Anisotropic scaffolds supported the enhanced migration of an invasive breast cancer cell line MDA-MB-231 with an altered spatial distribution of proliferative cells in contrast to invasive MDA-MB-468 and non-invasive MCF-7 cells lines. In addition, MDA-MB-468 showed increased migration upon epithelial-to-mesenchymal transition (EMT) in anisotropic scaffolds. The provision of controlled architecture in this system may act both to increase assay robustness and as a tuneable parameter to capture detection of a migrated population within a set time, with consequences for primary tumour migration analysis. The separation of invasive clones from a cancer biomass with *in vitro* platforms could enhance drug development and diagnosis testing by contributing assay metrics including migration rate, as well as modelling cell-cell and cell-matrix interaction in a system compatible with routine histopathological testing.

1. Introduction

The process of metastasis, whereby cancer cells are able to disengage from a primary tumour and seed and colonise distant sites of the body, remains the primary key contributor to cancer lethality. Cell migration, together with the ability to degrade extracellular matrix is a critical requirement for invasion [1] and could form a potential metric for assessing drug potency alongside indices of cell death. However, to date the development of robust migratory 3D models has received little attention [2]. In addition, cellular heterogeneity is a defining feature of the cancer microenvironment, and *in vitro* test systems that can distinguish or even separate cell types dependent on their migratory or invasive ability could contribute enhanced platforms for diagnosis or aid drug development [3]. *In vitro* cellular assays for examining cancer invasiveness and migratory potential within 3D extracellular matrices remain potent tools for examining features of this process [4,5], however such models now need adaptation into standardized and reproducible formats suitable for high-throughput applications [6]. If migration is to form a useful parameter for studies of cell behaviour and drug efficacy in this context, 3D models should be consistent with regard to fabrication and incorporate deterministic architecture to minimise random cell migration patterns.

The Boyden chamber assay, exploiting a chemokine gradient between upper and lower chambers to drive cell invasion and migration, can be readily adapted to model specific extracellular matrix (ECM) chemistries by simple coating procedures. However, a comprehensive assessment of three-dimensional cell invasion or migratory mechanisms using histological techniques is difficult to achieve in these systems, with metrics usually limited to an end-point summation of cell numbers within the lower chamber.

* Corresponding author.
E-mail address: ah492@cam.ac.uk (A. Husmann).
[1] Current address: LGC, Queen Road, Teddington, Middlesex, TW11 0LY, UK.
[2] Equal first authors.

Controlling the spatial distribution of cells on extracellular proteins at the 2D interface is challenging and we anticipate that with development, biomaterial platforms with controlled *x,y* and *z* internal dimensions could prove a valuable advance. Such platforms could additionally be engineered to confine cells in a more physiological context at the point of seeding, with better control of substrate chemistry. Furthermore, there is a physiological basis for the provision of anisotropic matrices in studies of this type. Other groups have shown previously that ECM surrounding human breast tumours can be remodelled to display spatially anisotropic features and a high degree of fibre orientation [7,8]. Further studies have shown that anisotropy enhances the invasion of cancer cells into the surrounding stroma and supports their eventual metastasis [9–11]. Therefore, whilst allowing for more controlled analyses of migration, the internal properties of our anisotropic scaffolds may recapitulate *in vivo* ECM conditions.

This group has previously described the formation of complex mammary tissue architectures [12,13] using mixtures of epithelial and stromal cells within collagen-based porous biomaterials with controlled architecture, achieved through an ice-templating process [14]. In the present study, we hypothesize that 3D collagen scaffolds with radially aligned anisotropic pores enhance the directed migration of invasive breast cancer cell lines over non-invasive phenotypes, thus providing a 3D natural substrate for interrogating invasive and migratory properties of cancer. To test our model, we generated scaffolds with splayed radially aligned pores or random isotropic porous architecture by a controlled freeze drying procedure [15,16]. We propose that this anisotropy could be achieved by modifying a previously established freeze drying method and manipulating ice crystal growth to produce scaffolds with orientated pores emanating from a central nucleation point. The freeze drying strategy utilised a spatially controlled thermal gradient from a single point source, acting both as a point of origin for ice growth and producing a moulded feature within the 3D structure allowing spatially repeatable seeding of a cell inoculate. We tested the capacity of the system to support directional cell migration by seeding a range of breast cancer cell lines exhibiting varied invasive characteristics on the basis of luminal or basal epithelial phenotype. Aliquots of MCF-7 (luminal A, non-invasive), MDA-MB-231 (triple negative, basal, claudin-low, invasive) or MDA-MB-468 (triple negative, basal, invasive) were used to evaluate scaffolds exhibiting either isotropic and anisotropic pore orientations. MDA-MB-468 cells were also treated to undergo an epithelial-to-mesenchymal transition (EMT) to verify whether this would influence migration potential in anisotropic scaffolds. As well as assessing the distribution of cells in a temporal context we also monitored cell proliferation within these systems by both EdU and Ki67 staining.

2. Materials and methods

2.1. Scaffold synthesis

All materials were obtained from Sigma Aldrich (Poole, UK), unless otherwise stated. Scaffolds were prepared according to a modified previously published method [15,16,17]. Collagen from bovine achilles tendon was dispersed overnight in 0.05 M acetic acid at 4° C to make a 1 wt% collagen slurry. The slurry was homogenised at about 10,000 rpm for 30 min using an overhead homogeniser, keeping the container in an ice water bath, followed by centrifugation at 2500 rpm for 5 min to remove air bubbles.

The slurry was carefully aspirated within the scaffold moulds (Fig. 1), taking care to completely cover the copper pins with minimal bubble formation before a plate of glass was applied to the top of the mould chamber. For anisotropic scaffolds, see also Table 1,

the freeze dryer shelf was cooled prior to use ensuring a shelf temperature of -40 °C. The moulds were placed so that the copper pins were in direct contact with the metal shelf. For isotropic scaffolds, the freeze dryer shelf was cooled from 20 °C to -40 °C over 1 h. The copper pins were thermally insulated with a thin rubber foam mat of less than 1 mm thickness so that they were not in direct thermal contact with the metal shelf. The freezing protocol was chosen to produce pore sizes around 100 μm away from the funnel [16]. Pore sizes in this range have been successfully used before [12,13].

Following freeze-drying, scaffolds were removed from the mould by carefully lifting the glass cover slide to which the collagen scaffolds stick very well. Scaffolds were immediately submerged in a cross-linking solution (70% ethanol + 33 mM 1-ethyl-3-(3-dimethylaminopropyl)-carbodiimide hydrochloride + 6 mM *N*-hydroxysuccinimide) for 30 min with constant agitation on a rotating plate. Following cross-linking, the scaffolds were removed to fresh 70% ethanol and degassed under vacuum (approximately 10 kPa) for 5 min. Samples were then stored in 70% ethanol to ensure sterility until needed.

2.2. Scanning electron microscopy

Scanning electron microscopy micrographs were used to visualise the pore structure of the scaffolds at various magnifications. Prior to imaging, collagen scaffolds were sputter coated with gold for 2 min at a current of 20 mA. All micrographs were taken on a JEOL 5800, with a tungsten source, operated at 10 kV.

2.3. X-ray micro-computed tomography

X-ray micro-computed tomography (μCT), Skyscan 1172, scans were taken of the whole scaffolds (25 kV, 140 μA). Reconstructions were performed with the software program NRecon (Skyscan), with a resolution of 6 μm.

2.4. Human breast cancer cell line culture

All cell lines were maintained between passages 5 to 15 in complete media as follows. MCF7 cells (ATCC) were cultured in DMEM media (Gibco, Life technologies) supplemented with 10% foetal bovine serum (FBS) (Gibco) in a humidified 5% CO_2 incubator at 37 °C. MDA-MB-468 and MDA-MB-231 were cultured in Leibovitz L-15 media (Gibco, 11415-064) supplemented with 10% FBS in
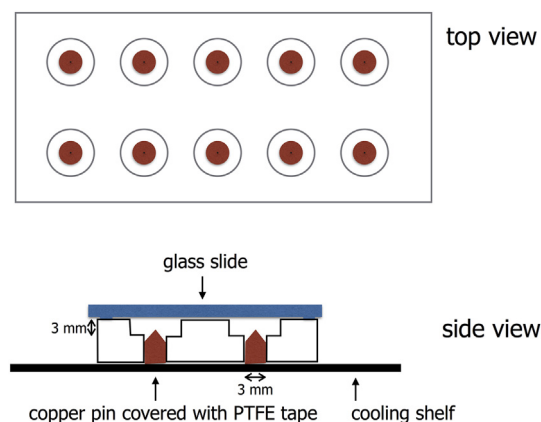

Fig. 1. The main body of the mould was machined from 9.6 mm thick polycarbonate sheet with evenly spaced 7 mm diameter by 3 mm deep troughs. In the centre of each trough, a 3 mm diameter hole was added in which a copper pin with a conical tip was inserted. The tip was covered by PTFE tape.

humidified air incubator at 37 °C.

2.5. Epithelial-to-mesenchymal transition induction of MDA-MB-468 cells

MDA-MB-468 cells were serum starved (0.5% FCS) and treated with 50 ng/ml epidermal growth factor (EGF) for 12 h as previously described [18]. EGF treatment continued for 10 days in normal conditions (10% FCS, Leibovitz, air incubator). Following this cells were either collected for western blotting, immunocytochemistry performed or seeded into anisotropic scaffolds for migration assays.

2.6. Sodium dodecyl sulphate - polyacrylamide gel electrophoresis (SDS-PAGE)/western blotting

EpH4 (negative control), MDA-MB-231 (positive control), MDA-MB-468 and MDA-MB-468 cells treated +EGF for 10d were collected in radio immunoprecipitation assay (RIPA) buffer. Bicinchronic acid assay (BCA) was performed and 20 μg protein was added per lane. Blots were blocked in 5% bovine serum albumin for 1 h. Primary antibodies vimentin (cell signalling, #5741, 1:1000) and loading control tubulin (abcam, ab6160, 1:10000) were diluted in blocking buffer and left rocking overnight 4₀C. Secondary antibodies anti-rabbit (Dako, PO448, 1:4000) and anti-rat (Dako,PO450, 1:2000) were diluted in blocking and left rocking at room temperature for 1 h.

2.7. Migration assay

Scaffolds were washed twice with sterile PBS followed by soaking overnight in the appropriate complete media supplemented with 50 μg/ml gentamicin (Sigma Aldrich, G1937), to ensure contamination free conditions. Using sterile forceps, scaffolds were moved into the upper wells of 6 mm diameter Boyden chambers (0.4 μm pore size, Corning) with upward facing seeding funnels. Care was taken to eliminate residual media from the scaffold. Migration assays were established under both serum gradient (upper chamber 1%/lower chamber 10%) and non-gradient (10%/10%) conditions for all cell types and scaffold architecture, using media optimised for each cell line as detailed above. Cells were trypsinized, checked for viability by Trypan blue exclusion assay (>90% in all cases) and resuspended in fresh complete media (1% FCS for gradient samples or 10% FCS for non-gradient samples (Fig. 2a)) at a concentration of 5×10^6 cells/ml with 5x pipette aspiration to minimise cell clumping on suspension. To characterise cell spreading at seeding, Countbright microbeads (Life technologies) were suspended alongside cells at a concentration of 5×10^3/mL. 10 μl (5×10^4 cells) of this cell/bead suspension was then pipetted into the nucleation point of each scaffold. The bottom chamber of the Boyden was then filled with 750 μl complete media (10% FCS is all cases) and the cells were left for 4 h to attach. The upper chamber was then filled with 250 μl media containing either 1% FCS for gradient samples or 10% FCS for non-gradient samples.

Samples were left to incubate for either 24hrs or 10 days, with media changed every 48hrs in the latter condition. In the 10 day samples, media was substituted for complete media containing 10 μM EdU for the final 24hrs, to quantify divided cells over that period. The provision of a serum gradient was provided to a subset of samples to test if a chemokine differential between upper and lower chambers of the supporting transwell plate was required to force cell migration within the scaffold depth. Following incubation, scaffolds were fixed for analysis in 4% paraformaldehyde overnight at 4 °C, washed in PBS and segmented in half through the nucleation point using a scalpel blade. One scaffold half was processed to paraffin for immunohistochemical analysis.

The provision of a serum gradient was provided to a subset of samples to test if a chemokine differential between upper and lower chambers of the supporting transwell plate was required to force cell migration within the scaffold depth.

2.8. Immunohistochemistry and imaging

Bisected scaffolds were washed in PBS and bathed directly in 2 μg/mL bisbenzimide-Hoechst 33342 (Thermofisher Scientific) for 10 min or for an assessment of cell proliferation stained for EdU incorporation according to the supplier's protocol (Click-iT, Thermofisher) before proceeding to Hoechst staining. The scaffolds were then washed in PBS 3 times and placed cut face down on a glass slide for fluorescence imaging. For immunohistochemical analysis paraffin sections were deparaffinised, rehydrated and boiled in 10 mM sodium citrate for antigen retrieval before blocking in 10% normal goat serum (Sigma) 0.05% triton-X PBS. Primary antibody Ki67 (ab15580, Abcam) was diluted 1:100 and incubated overnight at 4 °C in a humidified chamber. Signal was detected with conjugated secondary antibody AlexaFluor 647 (Invitrogen) diluted 1:500 and incubated for 1 h at room temperature. DNA was marked using Hoechst 33342 2 μg/mL (Thermofisher Scientific) for 10 min. Slides were mounted in PBS-glycerol 50:50 and viewed using confocal microscopy. Automated epifluorescent microscopy was carried out using a Zeiss Observer with 20× objective. Tile scans of $10 \times 8 \times 0.5$ mm (x,y,z dimensions) were performed to capture cells within the entire cut face of the scaffold presented to the slide.

2.9. Immunocytochemistry and imaging

MDA-MB-231, MDA-MB-468 and MDA-MB-468 + EGF were cultured on glass coverslips and fixed in 4% paraformaldehyde (PFA) for 10 min. Permeabilization was carried out for 15 min in 0.5% Triton-X/PBS followed by 1 h blocking in normal goat serum (NGS). Primary antibody anti-vimentin (cell signalling, #5741, 1:100) and negative control anti-rabbit IgG (Dako, XO936, 1:100) were diluted in blocking buffer and left overnight at 4 °C. Secondary goat anti-rabbit alexa fluor 488 (life technologies, A11008, 1:500) was applied to all samples for 1 h. DNA was marked using Hoechst and cells were visualized using epi-fluorescence. Using 3 separate fields of view all MDA-MB-468 cells (+/− EGF) were counted using

Table 1
Two distinct freeze-drying protocols were used to create scaffolds with either anisotropic or isotropic pore architectures. The difference was in the cooling procedure. In the anisotropic case, ice was nucleated at the pins from which it grew in directional channels. In the isotropic case, the slurry was cooled evenly. After ice was nucleated, it grew in a dendritic form throughout the slurry [16].

| Scaffold type	Cooling procedure	Freezing procedure	Subliming procedure
Anisotropic	Cooling shelf quenched to -40 °C moulds added when shelf was cold. Copper pins were in thermal contact with the cooling shelf.	Moulds were kept at -40 °C for 2 h to ensure complete freezing.	Ice was subliming for 18 h.
isotropic	Cooling shelf cooled from 20 °C to -40 °C in 1 h with moulds in situ, Copper pins were thermally insulated from the cooling shelf.	Moulds were kept at -40 °C for 2 h to ensure complete freezing.	Ice was subliming for 18 h.
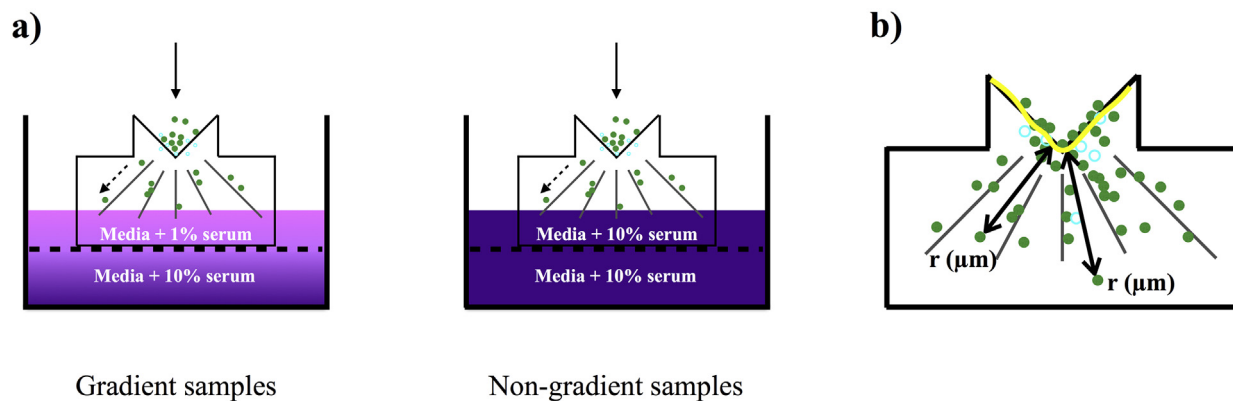
Fig. 2. (a) Scaffold seeding procedure consists of adding a mixture of cells (green) and beads (turquoise) into the funnel, for gradient samples and for non-gradient samples. (b) The distance travelled by the cell away from the funnel is measured as the shortest distance between the cell (in green) and the beads (in turquoise) with the line (in yellow) drawn along the funnel as seen under the microscope. (For interpretation of the references to colour in this figure legend, the reader is referred to the web version of this article.)

ImageJ. Following this vimentin positive cells were counted and a ratio of vimentin positive to all cells was calculated.

2.10. Statistical analysis

A Wilcoxon test on unpaired data of median distances, r_{median} (μm) (as measured according to the procedure shown in Fig. 2b), for each set-up was performed with a confidence value of 95% to check for statistically significant results. Relevant parameters were cell line type, scaffold type and vimentin expression.

3. Results

The fabrication of 3D collagen scaffolds combining functional internal anisotropic architecture with a defined funnel feature for repeatable cell seeding was confirmed by micro–computed tomography (μCT) and scanning electron microscopy (SEM) (Fig. 3). Scaffolds of the same external dimensions but with isotropic architecture could also be fabricated by varying the cooling protocol in the freeze drier (see Table 1). In both cases, pore size increased with depth away from the funnel. Both anisotropic and isotropic scaffolds exhibited a region with small isotropic pores immediately adjacent to the seeding funnel, a feature that may help with the retention of cells during assay setup and provide a barrier to test invasive qualities. The resultant isotropic architecture in both cases also gave seeded cells similar starting conditions. Beyond the funnel region, anisotropic scaffolds exhibited continuous elongated micro-porous architecture with a radial distribution within a conical shaped zone originating at the tip of the seeding funnel and extending to the base of the structure. In both scaffold types finer connections were evident in the macro-porous collagen walls indicating the presence of an inter-communicated structure.

24 h after seeding, a pooled assessment of data from all scaffolds and cell types demonstrated that 90% of cells were retained within 100 μm distance of the funnel, equating to approximately 0.03% of the scaffold full depth. Furthermore, it was noted from an analysis of sample median distance (r_{median}) from the funnel boundary, that beads and cells had a similar distribution at 24hr post-seeding (Fig. 4), indicating that cells and bead materials may interact and disperse in a similar manner at the nucleation point during setup. Distinguishing data by cell type, the tight localisation of MCF-7 and MDA-MB-468 cell lines to the funnel environment is evident, in contrast to the MDA-MB-231 cell line that had started to interact and spread within the scaffold by this time (Fig. 4). For 10 day data, see supplementary information S1.

Following 10 days of culture, we conclude that the median cell distance is significantly increased for MDA-MB-231 compared to either MDA-MB-468 or MCF7 samples using the Wilcoxon test on unpaired data (Fig. 5a). In addition, MDA-MB-231 cells displayed increased migration with the provision of an anisotropic scaffold, compared with isotropic conditions, and it was found that MDA-MB-231 cell migration was additionally supported by the provision of a serum gradient.

Indeed, complete migration of MDA-MB-231 cells to the base of the scaffold was often evident when both anisotropy and a serum gradient were applied (Fig. 5b), with a substantial population of cells occupying the full depth of the sample. All cell types displayed morphologies indicative of cells communicating with underlying substrate materials (Fig. 6) and an analysis of cell attachment to 2D cross-linked collagen films of the same material using brightfield and fluorescent microscopy revealed cell morphologies that closely reflected those observed on plastic slides (Fig. S2). Hersel et al. [19] report a biphasic relation between cell attachment and migration speed, which is in accordance with our observations that, while MDA-MB-468 and MCF7 cells attach well to collagen, they do not migrate as well as MDA-MB-231 cells.

Fig. 7a shows the spatial localisation of proliferating cells within the migrating cell populations by labelling dividing cells with EdU over the final 24hr of culture, and Fig. 7b correlates the median distances from the funnel for divided cells against the total cell population. Again, the extended migration capacity of the MDA-MB-231 cell line was evident against the other cell lines which could reflect their invasive capacity, and that this capacity was further supported within anisotropic scaffolds. There was a tendency for the median distances for the MDA-MB-231 EdU+ subset to be greater than bulk population values, indicating preferential division towards the leading edge of the migrating population. However, the ratio of non-dividing cells to dividing cells in MDA-MB-231 cultures was markedly lower than other cell types at approximately 10:1.

In order to further confirm the distribution of proliferating cells, we utilised immunohistochemical staining for another marker of proliferation, Ki67. Similar levels of proliferation were detected by each marker, see Supplementary Fig. S3, although there was a wider range of values with the EdU incorporation assay probably a reflecting the fact that EdU can only be incorporated into the DNA of cells during S phase whilst Ki67 is an expressed throughout the entire cell cycle in proliferating cells [20]. The distribution of proliferating MCF-7 and MDA-MB-468 cells is representative of the bulk population of cells that have stopped cycling. It is likely,
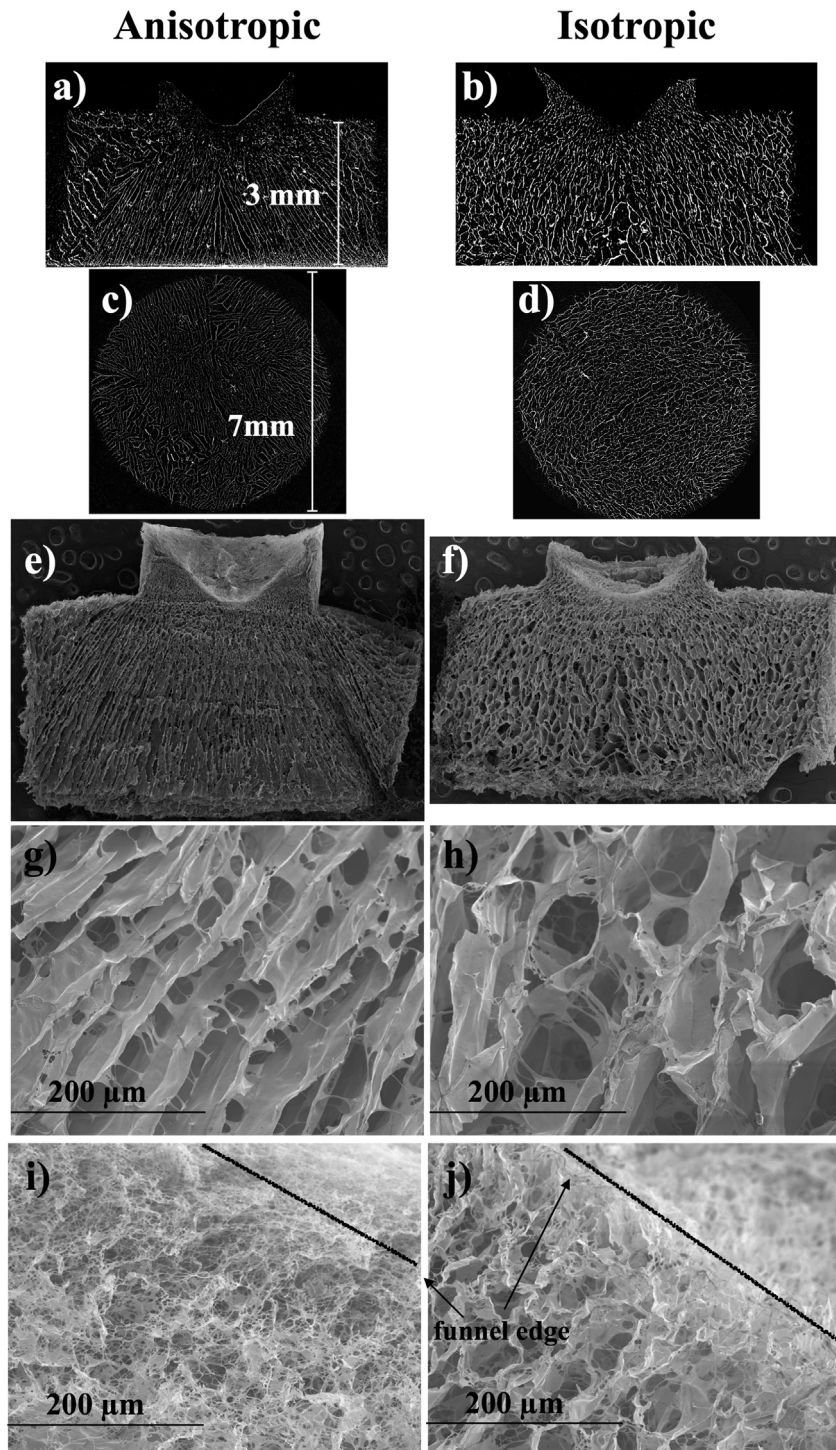
Anisotropic   Isotropic

Fig. 3. The scaffold architecture was visualized using micro–computed tomography (μCT) and scanning electron microscopy (SEM). (a–d) show reconstructed μCT pictures of transversal and horizontal cuts through an anisotropic and an isotropic scaffold. (e–j) show SEM pictures of the whole scaffold as well as a zoomed in part showing the different architectures and regions around the funnel.

therefore, that the controlled 3D architecture within our porous collagen scaffolds could provide a robust system for a spatial and quantitative analysis of cell migratory characteristics.

Confirmation that these scaffolds could distinguish invasive phenotypes was established by utilizing the properties of the MDA-MD-468 cell line. In separate experiments we induced an EMT by incubation in epidermal growth factor (see Fig. S4). Cells exposed to

EGF were seeded in anisotropic scaffolds together with control samples (untreated MDA-MD-468 cells) and a 10 day migration analysis was performed in the absence of a serum gradient in the same manner as earlier experiments. As shown in Fig. 8, it was observed that MDA-MD-468 cells with an induced mesenchymal phenotype migrated further within anisotropic scaffolds, indicating that these platforms could be used to monitor migratory features
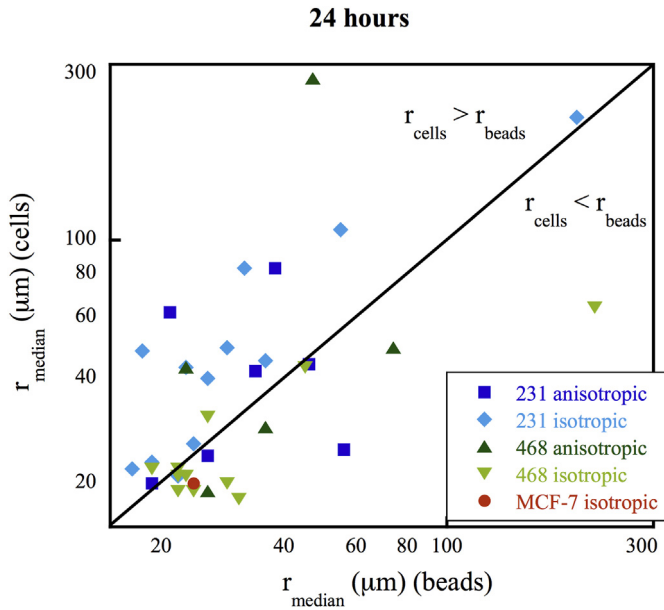
24 hours

Fig. 4. The mean distance travelled by the beads with respect to the mean distance travelled by the cells 24 h after seeding is plotted, colour coded by cell type and scaffold architecture. Each point represents one sample. (For interpretation of the references to colour in this figure legend, the reader is referred to the web version of this article.)

on an invasive cell phenotype.

4. Discussion

The development of new *in vitro* assays to monitor cell migration and invasion dynamics presents considerable challenges, many of which will have to be carefully controlled in order to increase assay robustness and repeatability. These include material selection and fabrication strategy, controlled cell dispersal at seeding within a 3D space and the establishment of biochemical or physical cues to encourage cell migration. Recently, the directional control of porous collagen architecture by ice-templating has been achieved [15–17]. We have shown in this paper that resultant pore orientation by ice-templating of a 3D cross-linked collagen scaffold can dictate cancer cell-line migration in 3D space, providing a permissible matrix to study cancer spread mechanisms in a system compatible with routine histopathological screening.

The provision of anisotropy resulted in enhanced directional migration of invasive MDA-MB-231 which exhibit a basal epithelial phenotype, in contrast to breast cancer lines displaying either mixed luminal/basal (MDA-MB-468) or luminal phenotype (MCF7), although this data was characterized by heterogeneity and long tail distributions. The provision of a 1%/10% serum gradient between the seeding funnel and lower chamber extended cellular migration supported by anisotropic architecture. Further, by inducing an EMT in the MDA-MB-468 cells line, a recognised mechanism for imparting invasive properties to normal and neoplastic cells [21,22], we observed that anisotropic architecture was able to support the migration of EGF exposed cells in preference to non-transformed controls.

Cancer cell lines as a collective group display the heterogeneity apparent within primary tumours [23] and it is reasonable to presume that a primary cell isolate would display migration characteristics in a range between the limits of the most invasive (MDA-MB-231) cells and least invasive (MCF7) cell lines in the current study. Both MDA-MB-468 and MDA-MB-231 lines are categorized
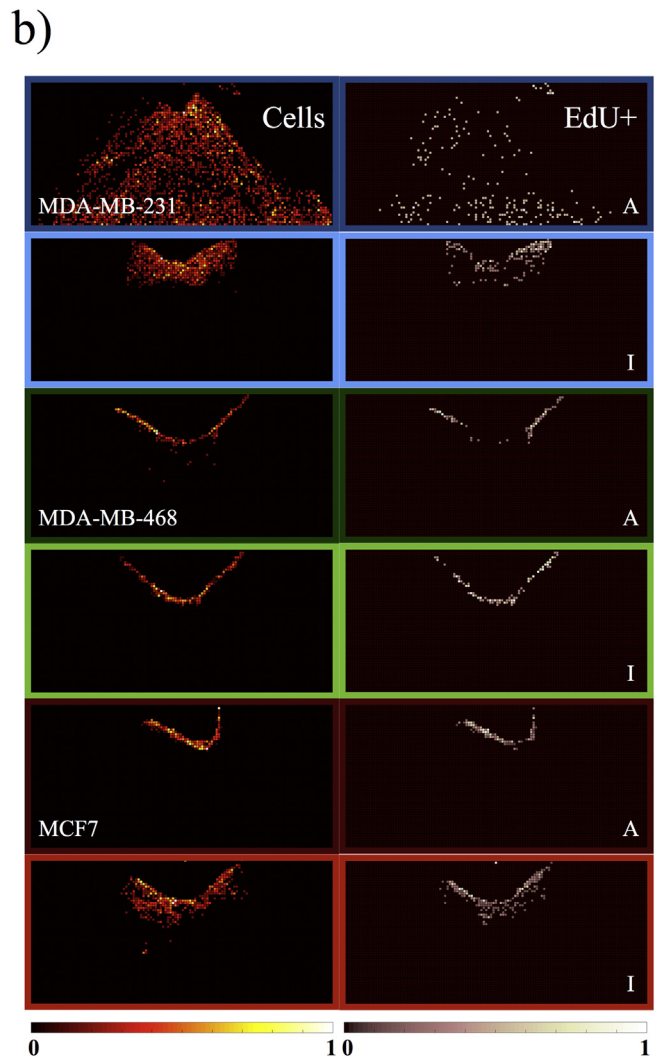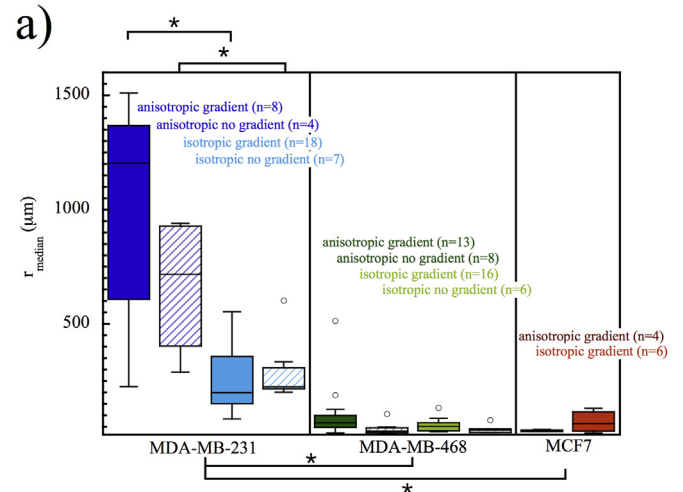

Fig. 5. (a) The distribution of the median cell distances after 10 days is shown sorted by cell type, scaffold architecture and whether or not a chemical gradient was present. In the case of the MDA-MB-231 samples, for the serum gradient and non-gradient conditions respectively, the scaffold architecture gives rise to a significant difference in median distance. In addition, the MDA-MB-231 cells migrate significantly further than the MDA-MB-468 and the MCF-7 cells. (b) Detailed heat maps of the distribution of cells within representative scaffolds, all with a chemical gradient applied, show marked differences in distribution with different cell types. Heat maps also show the distribution of the EdU labelled cells. A stands for anisotropic scaffolds, I for isotropic. Each heat map shows the full scaffold of 3.5 mm × 6 mm.
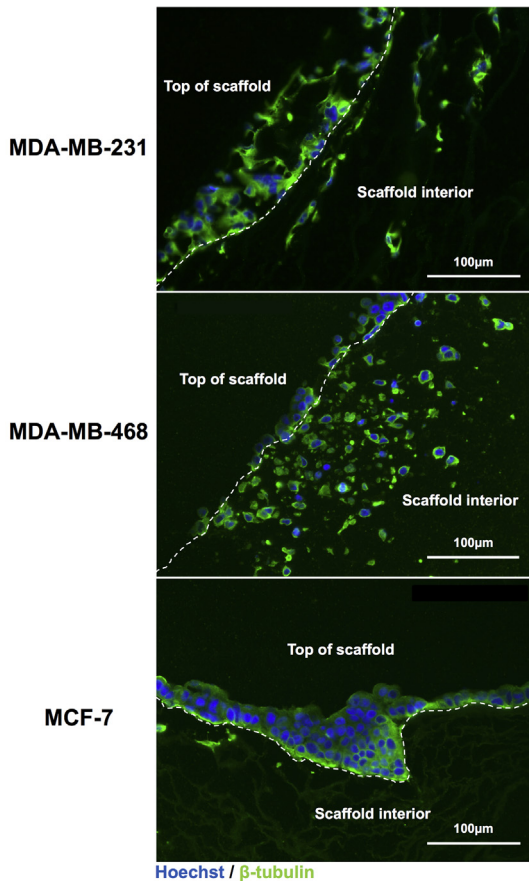
Fig. 6. MDA-MB-231, MDA-MB-468 and MCF7 cells show different morphologies in anisotropic collagen scaffolds. MDA-MB-231 cells migrate into the scaffold from the cell mass and have a thin spindle-like morphology. MDA-MB-468 cells migrate into the scaffold, disseminating from the cell mass as single cells/small cell clusters whilst maintaining a round morphology. MCF7 cells can be seen as a cell mass on top of the scaffold with few cells showing migration into the scaffold. Hoechst (blue) stains cell nuclei whilst β-tubulin (green) stains cell cytoskeleton components.

Fig. 7. (a) The log median distance of the cells marked with EdU is shown with respect to the log median distance of all cells. (b) The log of the total number of EdU marked cells is shown with respect to the log of the total number of cells in a sample.

as invasive [24], yet MDA-MB-468 retains epithelial characteristics under conditions of normoxia [25,26] and it is interesting that the current system likely supports the full-depth migration of only cell lines with mesenchymal properties, and invasive behaviour is a well characterized function of myoepithelial status [27]. The utility of the current study was further supported by observations that the migration of MDA-MB-468 cells was dependent on an EMT. Although these findings were observed with an induced EMT utilizing EGF, it is likely that further complex physical and biochemical cues operate within this system to support migration such as fluctuation in nutrient or dissolved oxygen concentration, both of which have been shown to modulate MDA-MB-231 cell migration [28].

Collagen type I is a pervasive stromal ECM species and a suitable candidate biomaterial for inclusion in cancer invasion and migration models. Indeed, cell exposure to underlying collagen type I has been highlighted as an important initiating event for cancer dissemination [29] and a 3D collagen type I lattice has been shown to up-regulate MMP2 expression [30], allowing cell-mediated modification of the substrate. Although collagen matrices *in vivo* are highly variable in their architecture [31], an analyses of collagen distribution around invading tumours in vivo has indicated that radially aligned fibres are pro-invasive compared with random
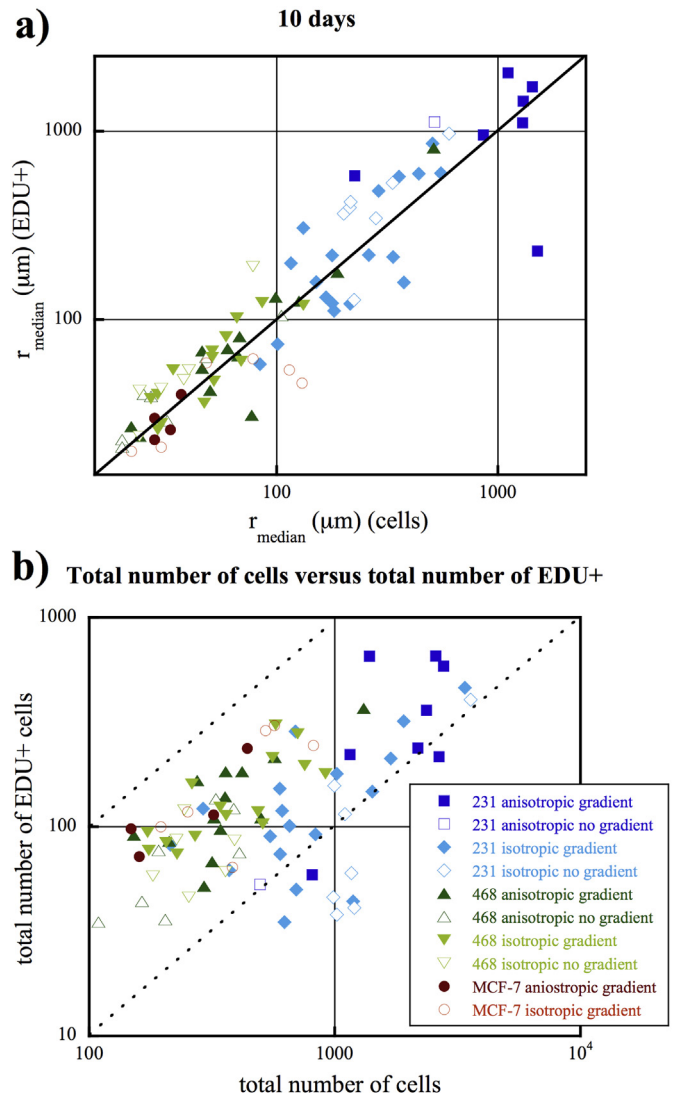
distributions, which are themselves remodelled to aligned fibres by invading cells [32]. Fibre alignment has also been shown to control the dispersal of T-cells [33]. In a similar manner, ECM fibre orientation has been shown to be permissive to breast carcinoma invasion [34] and directional cell elongation and motility guidance is a feature of 2D surfaces with anisotropic collagen fibres [35] although cell migration through 3D systems is a function of greater complexity including pore size [36] and nutrient diffusion [37]. It is likely that the perfusion of O_2, nutrients, cytokines and growth factors could be challenged towards the centre of large bulk materials, such as those employed in the current study, an effect compounded by static culture systems. The diffusion of factors will also be dictated by scaffold architecture, particularly with the provision of marked structural anisotropy which has been previously shown to support diffusion anisotropy [31].

The provision of a cross-linked porous scaffold system conveys advantages over preparations of collagen hydrogels used to coat trans-well membrane filters or as matrices for 3D cell dispersal and culture. The chemical properties of the collagen matrix can be varied [14,38] as well as the mechanical properties of such porous
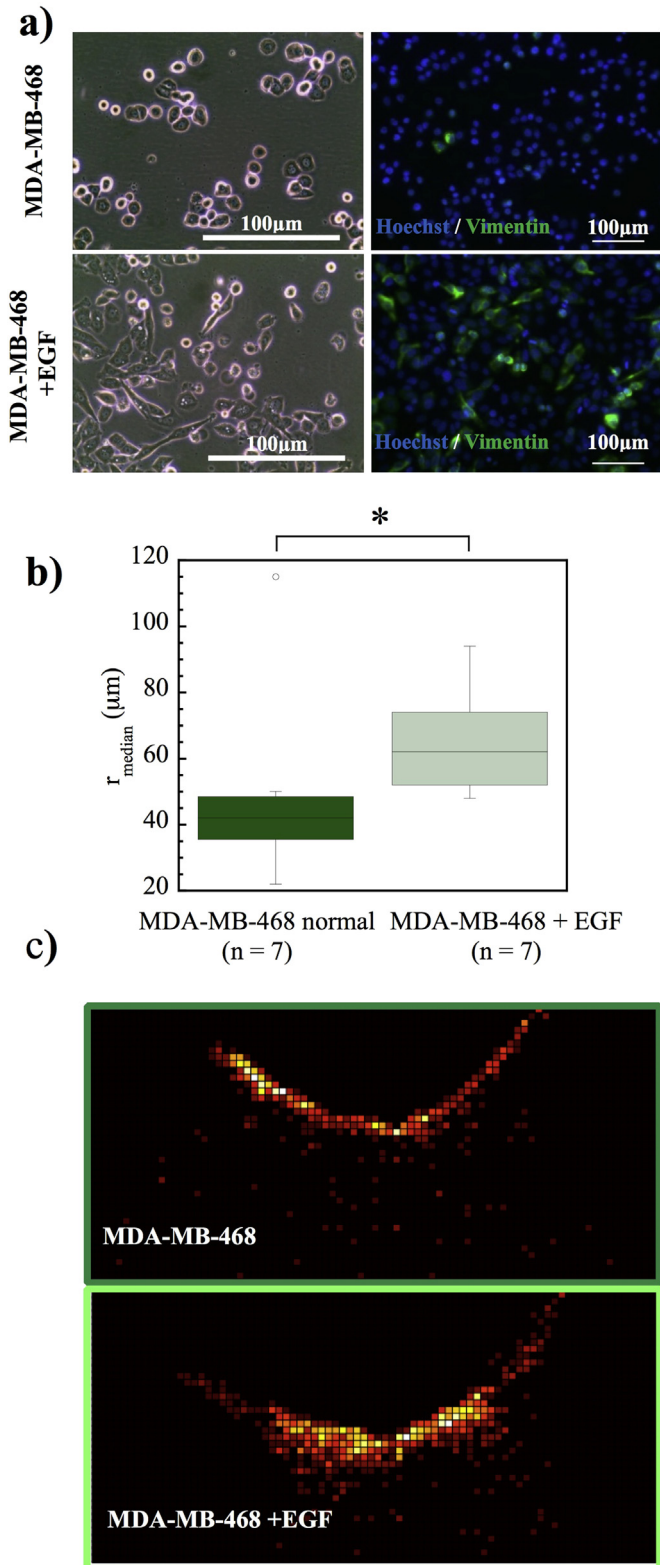
Fig. 8. MDA-MB-468 have increased migration potential in anisotropic collagen scaffolds after epithelial growth factor (EGF) mediated epithelial-mesenchymal transition (EMT) via signalling. a) Phase contrast image of MDA-MD-468 ± EGF and immunocytochemistry observation of vimentin expression. b) The distribution of the median cell distances after 10 days is shown between MDA-MD-468 ± EGF. There is a statistically significant difference between the two distributions by Wilcoxon test. c) Detailed heat maps of the distribution of cells within representative scaffolds show a more pronounced migration into the scaffold when EGF is present. Each heat map shows an area around the funnel of 2 mm × 4 mm.

networks which can be modulated by varying the cross-linking regime [39], whereas cell seeded bulk preparations of collagen are subject to cell-mediated remodelling and reorientation over short periods, alternating mechanical quantities and diffusion characteristics. Variance in substrate stiffness is an important consideration since stiffer ECMs are known to correlate with tumour invasive phenotypes, where they support focused cell adhesion complexes and enhanced ERK and Rho-kinase signalling [40].

Progressive tissue disorganisation has long been associated with aggressive cancer phenotypes and anisotropic spatial arrangements of collagen perpendicular to breast tumour mass are associated with poor outcome [41]. A system for controlling biomaterial substrate organisation may enable the provision of *in vitro* cell culture tools for informed clinical diagnoses. Furthermore, controlling internal geometry may offer a tuneable mechanism to detect invasive capability in a seeded cell population, allowing the earlier detection of migrated phenotypes and, if radial in alignment, allowing the ordered presentation of new surfaces to a migrating and proliferating cell mass enhancing cell monitoring and data analysis. With modification such substrates may even aid the detection or selection of invasive clones from a heterogeneous cell population when applied to an analysis of primary tumour samples. Furthermore, cancer cell lines are known to adopt a distinct morphology in 3D culture that correlates with invasive profile [42] and attempting to monitor invasion and migration from this 3D ground-state may be more reflective of invasive ability in vivo. It is noteworthy that in certain cancer cell lines, signalling pathways that control cell polarity and resultant tissue architecture, for example the differential regulation of integrin beta1 and EGFR status, are dependent on the three-dimensional state of tissues [43].

The precise replication of the *in vivo* ECM environment is an ideal target for the development of model systems although to satisfy assay robustness such systems should be as replicable as possible. It is recognised that, in the absence of stromal cells [44], reconstituted basement membrane (rBM) is required for establishing polar epithelial morphology [45], and the ability to break through this barrier is a key determinant of invasion. The deployment of rBM for high-throughput *in vitro* assays is not practical considering its susceptibility to batch variation and tumorigenic origin [46]. We have previously demonstrated the utility of pure collagen and hyaluronic acid blended collagen for the development of mammary tissue structures with functional attributes [12,13]. The provision of a scaffold that is capable of supporting normal tissue architecture or physiological developmental processes such as collective cell migration [47] seen in mammary gland formation and other tissues, would be an important advantage to such systems, and would enable the *in vitro* study of cancer cell spread within a relevant context.

In the current study, we have manufactured collagen structures that include defined seeding points for cells. We additionally employed synthetic micro-beads to aid our study of cell spreading characteristics within the nucleation point at seeding and to act as a point of reference for normalising the cell spread data within these freely permeable systems. It is noteworthy that these data revealed similar spread characteristics for both cells and beads at 24hr post-seeding although it was observed that bead spread was increased during the 10 day culture period indicating that beads were susceptible to mechanical or cell manipulation during the procedure. It is likely that the inclusion of normalisation or calibrator materials and methodology would be a requirement for process automation and quality control. Likewise fabrication strategies requiring only minimal further processing steps are beneficial to manufacturability. It is conceivable that the integration of sample preparation,

culture and processing could create automated systems for high-throughput migration analysis. Coupled to developments in scaffold materials to enable imaging to depth, such systems could provide real-time platforms for cell migration analytics.

5. Conclusions

The development of more informative 3D *in vitro* assays of cancer cell invasion and migration, amenable to high-throughput analyses with increased reproducibility, may advance current *in vitro* methods for assessing cancer cell invasiveness and migratory status. Anisotropic collagen scaffolds were readily able to support the full depth migration of the basal epithelial invasive cell line MDA-MB-231 over a 10 day time period and to differentiate MDA-MB-468 cells on the basis of an induced invasive phenotype by exposure to EGF, demonstrating the utility for such structures for distinguishing these features *in vitro*.

Acknowledgments

Appendix A. Supplementary data

Supplementary data related to this article can be found at http://dx.doi.org/10.1016/j.biomaterials.2016.10.048.

References

[1] J. Yang, S.A. Mani, J.L. Donaher, S. Ramaswamy, R.A. Itzykson, C. Come, P. Savagner, I. Gitelman, A. Richardson, R.A. Weinberg, Twist, a master regulator of morphogenesis, plays an essential role in tumor metastasis, Cell 117 (2004) 927—939.

[2] J. Steinwachs, C. Metzner, K. Skodzek, N. Lang, I. Thievessen, C. Mark, S. Münster, K.E. Aifantis, B. Fabry, Three-dimensional force microscopy of cells in biopolymer networks, Nat. Meth. 13 (2016) 171—176.

[3] C. Decaestecker, O. Debeir, P. Van Ham, R. Kiss, Can anti-migratory drugs be screened in vitro? A review of 2D and 3D assays for the quantitative analysis of cell migration, Med. Res. Rev. 27 (2007) 149—176.

[4] C.S. Szot, C.F. Buchanan, J.W. Freeman, M.N. Rylander, 3D in vitro bioengineered tumors based on collagen I hydrogels, Biomaterials 32 (2011) 7905—7912.

[5] C. Lovitt, T. Shelper, V. Avery, Advanced cell culture techniques for cancer drug discovery, Biol. (Basel) 3 (2014) 345—367.

[6] M. Alemany-Ribes, C.E. Semino, Bioengineering 3D environments for cancer models, Adv. Drug. Deliv. Re 79—80 (2014) 1—10.

[7] R. Jiang, X. Zeng, S. Sun, Z. Ma, X. Wang, Assessing detection, discrimination, and risk of breast cancer according to anisotropy parameters of diffusion tensor imaging, Med. Sci. Monit. 22 (2016) 1318—1328.

[8] S. Kakkad, J. Zhang, A. Akhbardeh, D. Jacob, B. Krishnamachary, M. Solaiyappan, M.A. Jacobs, V. Raman, D. Leibfritz, K. Glunde, Z.M. Bhujwalla, Collagen fibers mediate MRI-detected water diffusion and anisotropy in breast cancers, Neoplasia 18 (10) (2016) 585—593.

[9] M.W. Conklin, P.J. Keely, Why the stroma matters in breast cancer, Cell. adh. Migr. 6 (3) (2012) 249—260.

[10] P.P. Provenzano, D.R. Inman, K.W. Eliceiri, J.G. Knittel, L. Yan, C.T. Rueden, J.G. White, P.J. Keely, Collagen density promotes mammary tumor initiation and progression, BMC Med. 6 (2008) 11.

[11] P. Schedin, P.J. Keely, The mammary gland as an experimental model: mammary gland ECM remodeling, stiffness, and mechanosignaling in normal development and tumor progression, Cold Spring Harb. Perspect. Biol. 3 (2011) 1.

[12] J.J. Campbell, N. Davidenko, M.M. Caffarel, R.E. Cameron, C.J. Watson, A multifunctional 3D Co-Culture system for studies of mammary tissue morphogenesis and stem cell biology, PLoS One 6 (2011).

[13] J.J. Campbell, L.A. Botos, T.J. Sargeant, N. Davidenko, R.E. Cameron, C.J. Watson, A 3-D in vitro co-culture model of mammary gland involution, Integr. Biol. (Camb) 6 (2014) 618—626.

[14] N. Davidenko, J.J. Campbell, E.S. Thian, C.J. Watson, R.E. Cameron, Collagen-hyaluronic acid scaffolds for adipose tissue engineering, Acta Biomater. 6 (2010) 3957—3968.

[15] K.M. Pawelec, A. Husmann, S. Best, R.E. Cameron, A design protocol for tailoring ice-templated scaffold structure, J. R. Soc. Interface 11 (2014) 92.

[16] A. Husmann, K. Pawelec, C. Burdett, S. Best, R. Cameron, Numerical simulations to determine the influence of mould design on ice-templated scaffold structures, J. Bio. Eng. Info 1 (2015) 47.

[17] N. Davidenko, T. Gibb, C. Schuster, S.M. Best, J.J. Campbell, C.J. Watson, R.E. Cameron, Biomimetic collagen scaffolds with anisotropic pore architecture, Acta Biomater. 8 (2012) 667—676.

[18] F.M. Davis, M.T. Parsonage, P.J. Cabot, M.O. Parat, E.W. Thompson, S.J. Roberts-Thomson, G.R. Monteith, Assessment of gene expression of intracellular calcium channels, pumps and exchangers with epidermal growth factor-induced epithelial-mesenchymal transition in a breast cancer cell line, Cancer Cell Int. 13 (1) (2013) 76.

[19] U. Hersel, C. Dahmen, H. Kessler, RGD modified polymers: biomaterials for stimulated cell adhesion and beyond, Biomaterials 24 (2003) 4385—4415.

[20] N. Kee, S. Sivalingam, R. Boonstra, J.M. Wojtowicz, The utility of Ki-67 and BrdU as proliferative markers of adult neurogenesis, J. Neurosci. Methods 115 (1) (2002) 97—105.

[21] M.A. Huber, N. Kraut, H. Beug, Molecular requirements for epithelial—mesenchymal transition during tumor progression, Curr. Opin. Cell Biol. 17 (5) (2005) 548—558.

[22] J.P. Thiery, H. Acloque, R.Y.J. Huang, M.A. Nieto, Epithelial-mesenchymal transitions in development and disease, Cell 139 (5) (2009) 871—890.

[23] P.J. Keller, A.F. Lin, L.M. Arendt, I. Klebba, A.D. Jones, J.A. Rudnick, T.A. DiMeo, H. Gilmore, D.M. Jefferson, R.A. Graham, S.P. Naber, S. Schnitt, C. Kuperwasser, Mapping the cellular and molecular heterogeneity of normal and malignant breast tissues and cultured cell lines, Breast Cancer Res. 12 (5) (2010).

[24] K.J. Cheung, E. Gabrielson, Z. Werb, A.J. Ewald, Collective invasion in breast cancer requires a conserved basal epithelial program, Cell 155 (7) (2013).

[25] F.M. Davis, I. Azimi, R.A. Faville, A.A. Peters, K. Jalink, J.W. Putney Jr., G.J. Goodhill, E.W. Thompson, S.J. Roberts-Thomson, G.R. Monteith, Induction of epithelial—mesenchymal transition (EMT) in breast cancer cells is calcium signal dependent, Oncogene 33 (2013) 2307—2316.

[26] M. Jo, R.D. Lester, V. Montel, B. Eastman, S. Takimoto, S.L. Gonias, Reversibility of epithelial-mesenchymal transition (EMT) induced in breast cancer cells by activation of urokinase receptor-dependent cell signaling, J. Biol. Chem. 284 (2009) 22825—22833.

[27] L.A. Gordon, K.T. Mulligan, H. Maxwell-Jones, M. Adams, R.A. Walker, J.L. Jones, Breast cell invasive potential relates to the myoepithelial phenotype, Int. J. Cancer 106 (2003) 8—16.

[28] A. Nagelkerke, J. Bussink, H. Mujcic, B.G. Wouters, S. Lehmann, F.C. Sweep, P.N. Span, Hypoxia stimulates migration of breast cancer cells via the PERK/ATF4/LAMP3-arm of theunfolded protein response, Breast Cancer Res. 15 (2013).

[29] K.V. Nguyen-Ngoc, K.J. Cheung, A. Brenot, E.R. Shamir, R.S. Gray, W.C. Hines, P. Yaswen, Z. Werb, A.J. Ewald, ECM microenvironment regulates collective migration and local dissemination in normal and malignant mammary epithelium, P. Natl. Acad. Sci. U. S. A. 109 (2012) 2595—2604.

[30] C. Guo, L. Piacentini, Type I collagen-induced MMP-2 activation coincides with up-regulation of membrane type 1-matrix metalloproteinase and TIMP-2 in cardiac fibroblasts, J. Biol. Chem. 278 (2003) 46699—46708.

[31] T. Stylianopoulos, B. Diop-Frimpong, L.L. Munn, R.K. Jain, Diffusion anisotropy in collagen gels and tumors: the effect of fiber network orientation, Biophys. J. 99 (2010) 3119—3128.

[32] P.P. Provenzano, K.W. Eliceiri, J.M. Campbell, D.R. Inman, J.G. White, P.J. Keely, Collagen reorganization at the tumor-stromal interface facilitates local invasion, BMC Med. 4 (2006) 38.

[33] H. Salmon, F. Franciszkiewicz, D. Damotte, M.C. Dieu-Nosjean, P. Validire, A. Trautmann, F. Mami-Chouaib, E. Donnadieu, Matrix architecture defines the preferential localization and migration of T cells into the stroma of human lung tumors, J. Clin. Invest. 122 (2012) 899—910.

[34] N. Yang, R. Mosher, S. Seo, D. Beebe, A. Friedl, Syndecan-1 in breast cancer stroma fibroblasts regulates extracellular matrix fiber organization and carcinoma cell motility, Am. J. Pathol. 178 (2011) 325—335.

[35] K. Poole, K. Khairy, J. Friedrichs, C. Franz, D.A. Cisneros, J. Howard, D. Mueller, Molecular-scale topographic cues induce the orientation and directional movement of fibroblasts on two-dimensional collagen surfaces, J. Mol. Biol. 349 (2005) 380—386.

[36] K. Wolf, S. Alexander, V. Schacht, L.M. Coussens, U.H. von Andrian, J. van Rheenen, E. Deryugina, P. Friedl, Collagen-based cell migration models in vitro and in vivo, Semin. Cell Dev. Biol. 20 (2009) 931—941.

[37] B.A. Harley, H.D. Kim, M.H. Zaman, I.V. Yannas, D.A. Lauffenburger, L.J. Gibson, Microarchitecture of three-dimensional scaffolds influences cell migration behavior via junction interactions, Biophys. J. 95 (2008) 4013—4024.

[38] M.J. Sherratt, D.V. Bax, S.S. Chaudhry, N. Hodson, J.R. Lu, P. Saravanapavan, C.M. Kielty, Substrate chemistry influences the morphology and biological function of adsorbed extracellular matrix assemblies, Biomaterials 26 (34) (2005) 7192—7206.

[39] C.N. Grover, J.H. Gwynne, N. Pugh, S. Hamaia, R.W. Farndale, S.M. Best, R.E. Cameron, Crosslinking and composition influence the surface properties, mechanical stiffness and cell reactivity of collagen-based films, Acta Biomater. 8 (2012) 3080—3090.

[40] M.J. Paszek, N. Zahir, K.R. Johnson, J.N. Lakins, G.I. Rozenberg, A. Gefen, C.A. Reinhart-King, S.S. Margulies, M. Dembo, D. Boettiger, D.A. Hammer, V.M. Weaver, Tensional homeostasis and the malignant phenotype, Cancer Cell 8 (2005) 241–254.

[41] K.M. Riching, B.L. Cox, M.R. Salick, C. Pehlke, A.S. Riching, S.M. Ponik, B.R. Bass, W.C. Crone, Y. Jiang, A.M. Weaver, K.W. Eliceiri, P.J. Keely, 3D collagen alignment limits protrusions to enhance breast cancer cell persistence, Biophys. J. 107 (2014) 2546–2558.

[42] P.A. Kenny, G.Y. Lee, C.A. Myers, R.M. Neve, J.R. Semeiks, P.T. Spellman, K. Lorenz, E.H. Lee, M.H. Barcellos-Hoff, O.W. Petersen, J.W. Gray, M.J. Bissell, The morphologies of breast cancer cell lines in three-dimensional assays correlate with their profiles of gene expression, Mol. Oncol. 1 (2007) 84–96.

[43] J. Debnath, J.S. Brugge, Modelling glandular epithelial cancers in three-dimensional cultures, Nat. Rev. Cancer 5 (2005) 675–688.

[44] T. Gudjonsson, L.R. ønnov-Jessen, R. Villadsen, F. Rank, M.J. Bissell, O.W. Petersen, Normal and tumor-derived myoepithelial cells differ in their ability to interact with luminal breast epithelial cells for polarity and basement membrane deposition, J. Cel. Sci. 115 (2002) 39–50.

[45] C.M. Nelson, M.J. Bissell, Of extracellular matrix, scaffolds, and signaling: tissue architecture regulates development, homeostasis, and cancer, Annu. Rev. Cell Dev. Biol. 22 (2006) 287–309.

[46] D.W. Hutmacher, D. Loessner, S. Rizzi, D.L. Kaplan, D.J. Mooney, J.A. Clements, Can tissue engineering concepts advance tumor biology research? Trends Biotechnol. 28 (3) (2010) 125–133.

[47] A. Ewald, B. Chan, Collective epithelial migration and cell rearrangements drive mammary branching morphogenesis, Dev. Cell 14 (2008) 570–581.